

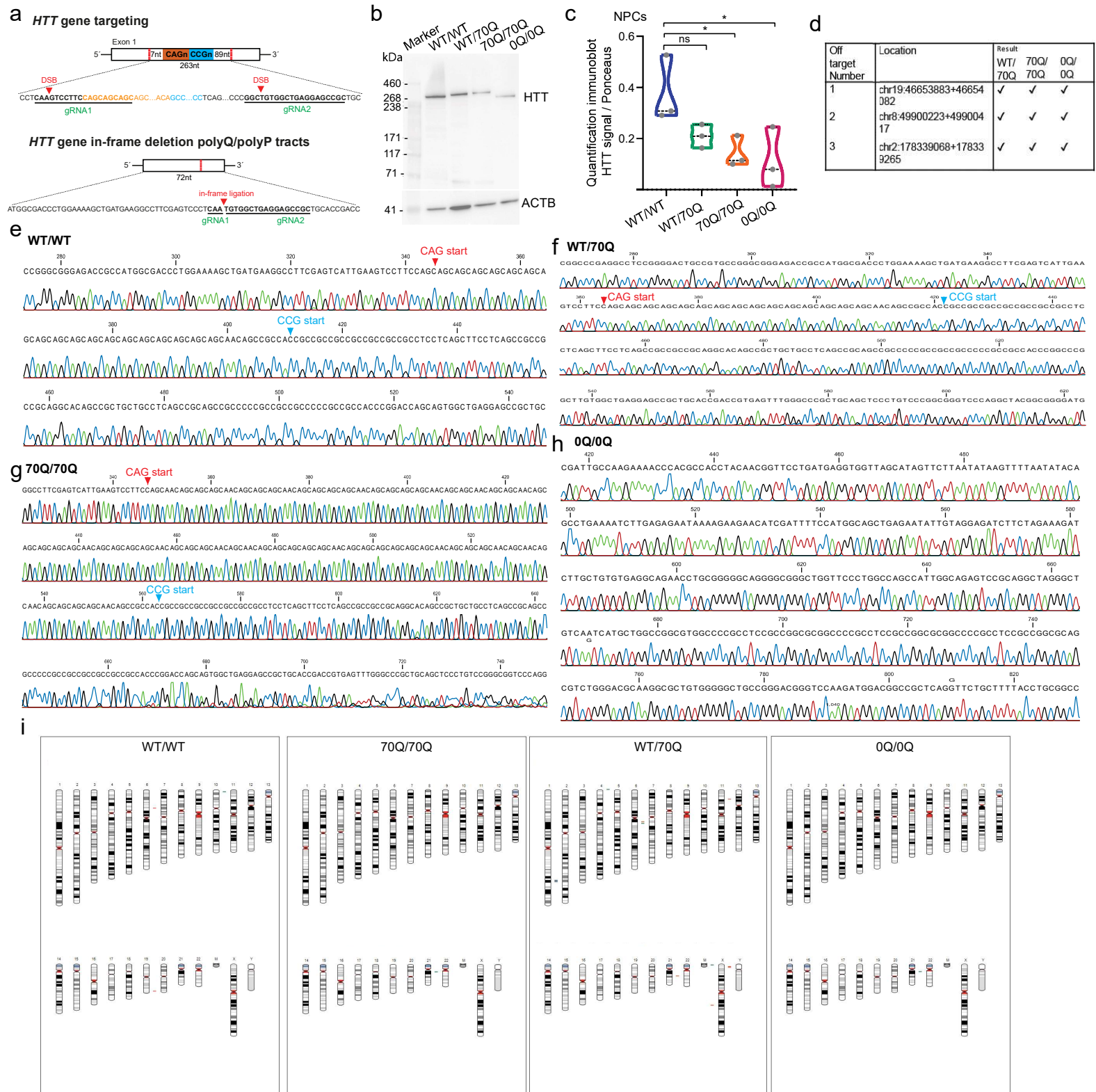
SUPPLEMENTARY INFORMATION

Mutant huntingtin impairs neurodevelopment in human brain organoids through CHCHD2-mediated neurometabolic failure

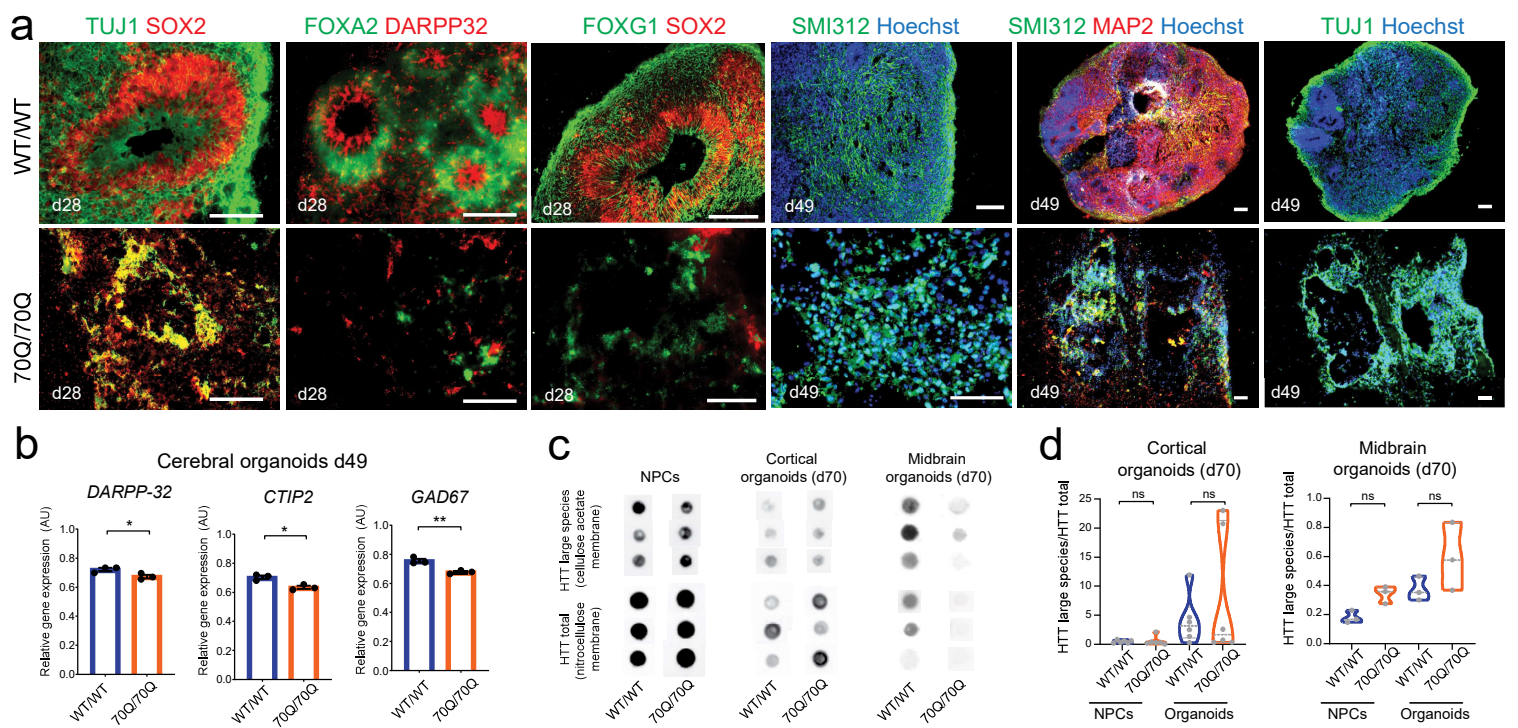
Lisowski, Lickfett et al.

Manuscript correspondence:

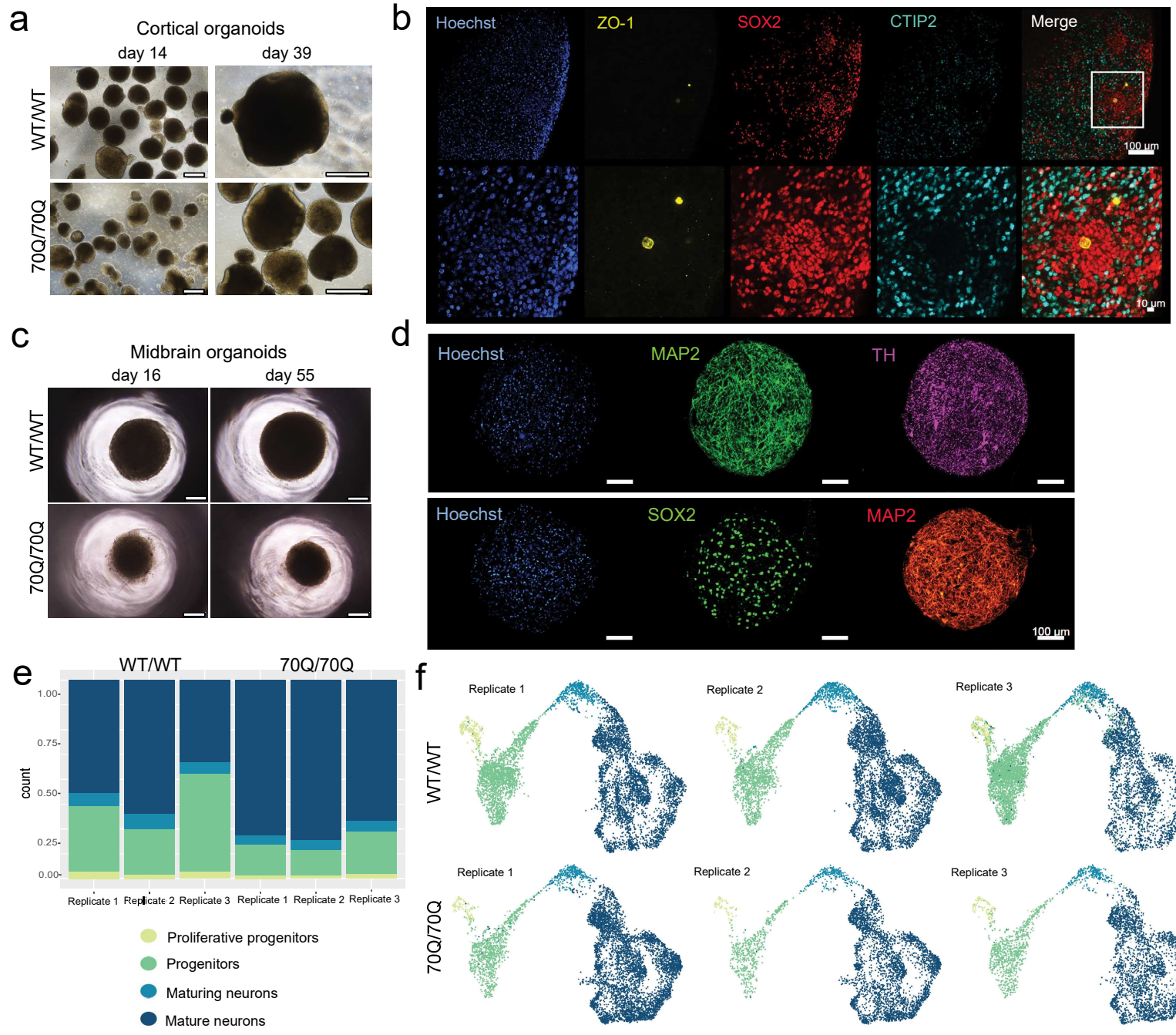
Alessandro Prigione, alessandro.prigione@hhu.de



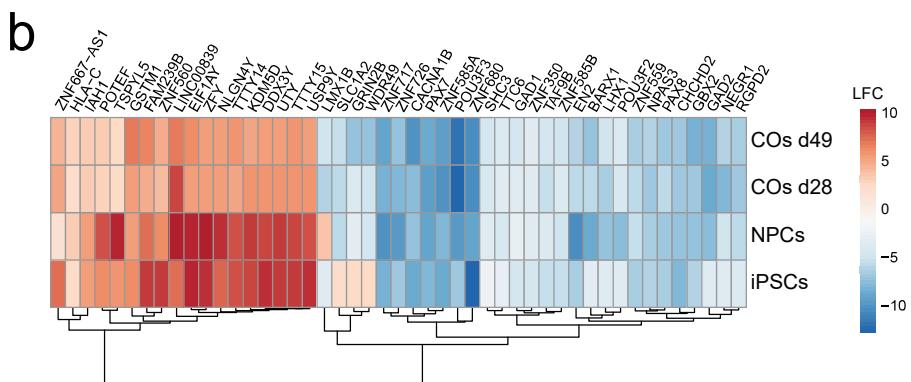
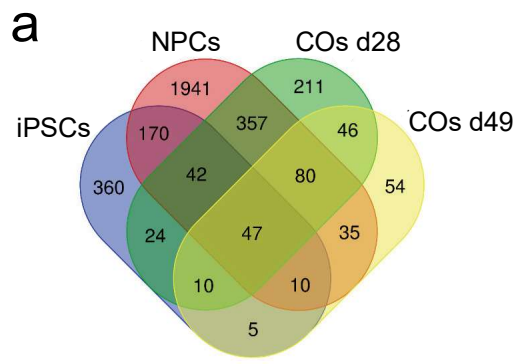
Supplementary Fig. 1. Characterization of engineered isogenic iPSCs carrying mHTT (related to Fig. 1). **a** Schematics of *HTT* gene targeting. DSB: double-strand breaks, gRNAs: guide RNAs. **b** Representative immunoblot of engineered isogenic NPCs using anti-Huntingtin antibody (ab109115). The results were confirmed in 3 independent experiments. **c** Quantification of HTT immunoblot in NPCs. n=3 independent biological replicates (dots) per line; *p<0.05, ns: not significant; unpaired two-tailed Welch t test. **d** Off-target analysis of top three predicted sites by CRISPOR. Analysis in the engineered iPSC lines (WT/70Q, 70Q/70Q, 0Q/0Q) did not show sequence alterations. **e-h** Sanger sequencing of target *HTT* region including indication of CAG starting site (in red) and CCG starting site (in blue). Images show the wild-type allele for WT/WT and WT/70Q iPSCs, one mutant allele for 70Q/70Q iPSCs, and one allele for 0Q/0Q iPSCs. **i** Normal karyotype assessed by SNP karyotyping (visualized with KaryoStudio v1.4) in WT/WT iPSCs and in the derived engineered lines (WT/70Q, 70Q/70Q, 0Q/0Q).



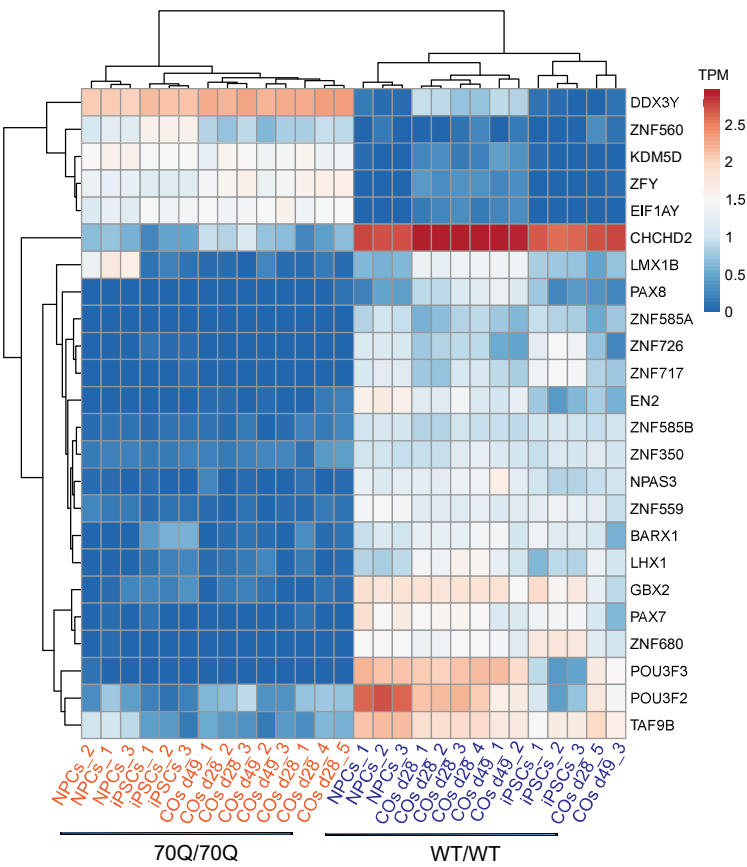
Supplementary Fig. 2. Analysis of brain organoids carrying mHTT (related to Fig. 1 and Fig. 2). **a** Immunostaining of unguided cerebral organoids at day 28 and 49 showing defective cytoarchitecture and neural progenitor cell (NPC) organization in 70/70Q. Data were repeated in three independent experiments. Scale bar: 100 μ m. **b** qPCR analysis of neuronal markers in unguided cerebral organoids at day 49. Mean +/- s.e.m.; n=3 independent biological replicates (dots) per line (AU=arbitrary units); *p<0.05 **p<0.01; unpaired two-tailed t test. Four organoids were pooled for each individual RNA isolation. **c-d** Representative images and related quantification of filter retardation assay (FRA) in NPCs and in guided region-specific brain organoids (cortical and midbrain) to assess the potential presence of HTT protein aggregates using anti-Huntingtin antibody (ab109115). Cellulose acetate membranes were used to visualize aggregated HTT protein species, and nitrocellulose membrane to visualize total HTT protein species. n=3 independent biological replicates (dots) per line; ns: not significant; unpaired two-tailed t test.



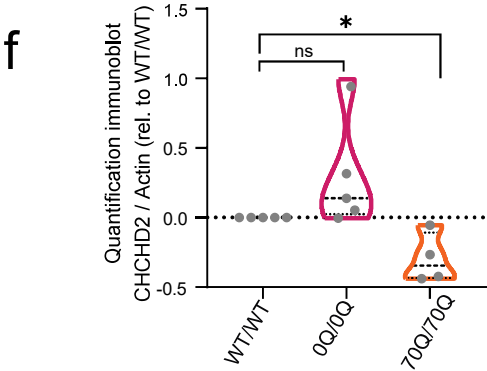
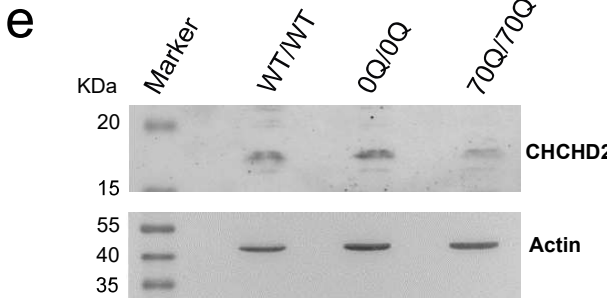
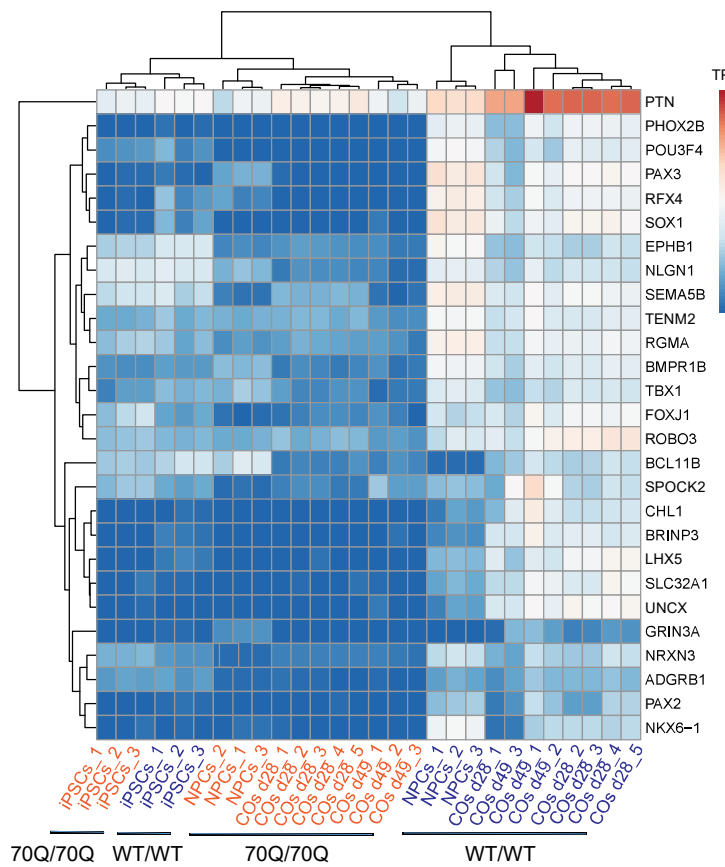
Supplementary Fig. 3. Guided region-specific brain organoids carrying mHTT (related to Fig. 2). **a** Representative images of cortical organoids visualized with bright field microscope. Data were repeated in three independent experiments. Scale bar: 400 μ m. **b** Immunostaining of cortical organoids at day 35 showing the presence of progenitor and neuronal and cortical markers. Data were repeated in two independent experiments. Scale bar: 100 μ m (above), 10 μ m (below). **c** Representative images of midbrain organoids visualized with bright field microscope. Data were repeated in three independent experiments. Scale bar: 200 μ m. **d** Immunostaining of midbrain organoids at day 35 showing the presence of progenitor and neuronal and dopaminergic markers. Data were repeated in two independent experiments. Scale bar: 100 μ m. **e** Single-cell RNA sequencing-based quantification of the four annotated cell populations in three biological replicates (each containing 48 individual organoids) of midbrain organoids from WT/WT and 70Q/70Q. **f** UMAP analysis showing the overall cell composition of the four populations distribution in biological replicates of midbrain organoids from WT/WT and 70Q/70Q.



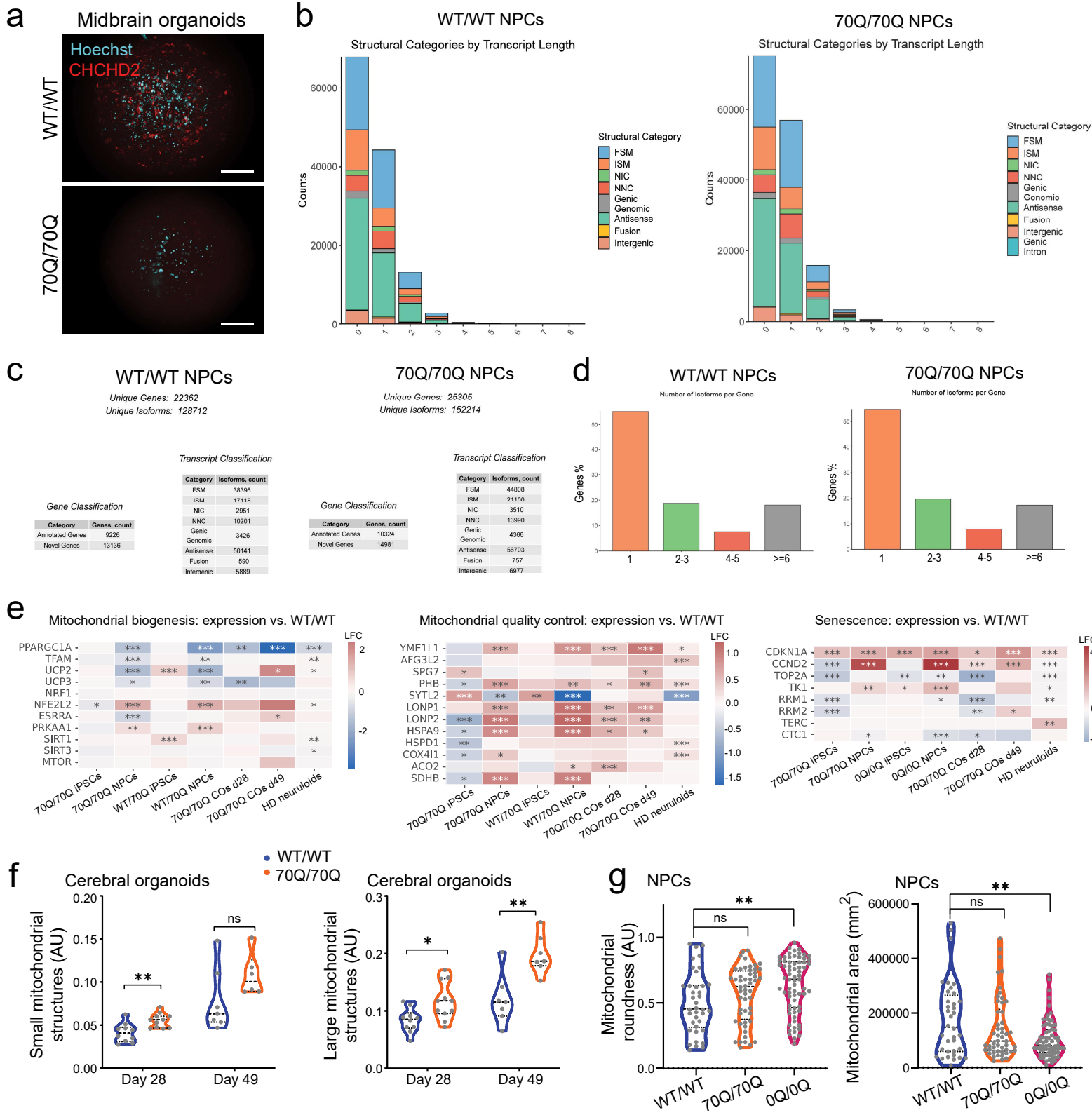
C Nucleic acid binding genes



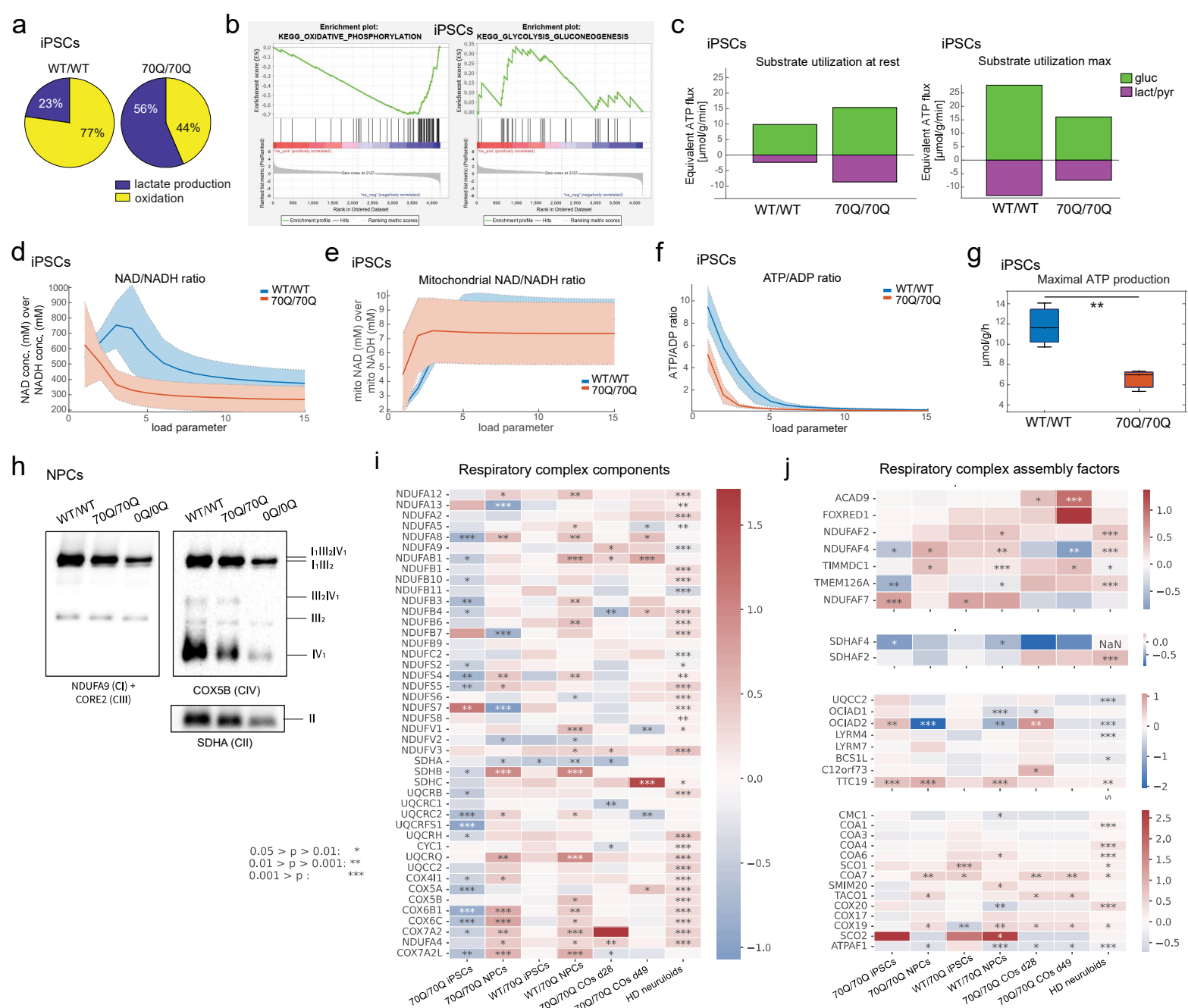
d Nervous system development genes



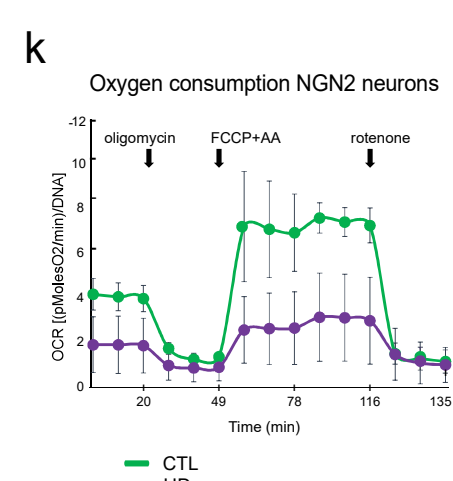
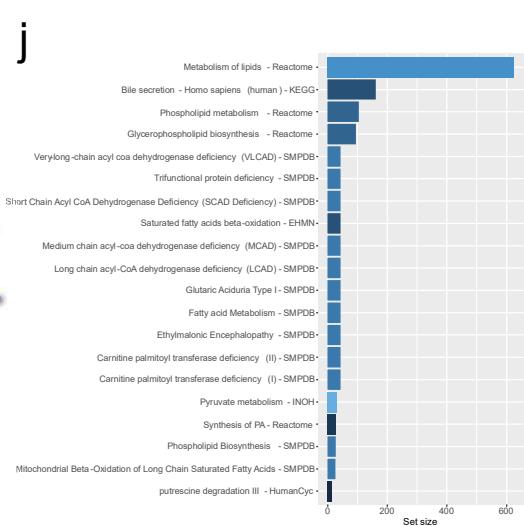
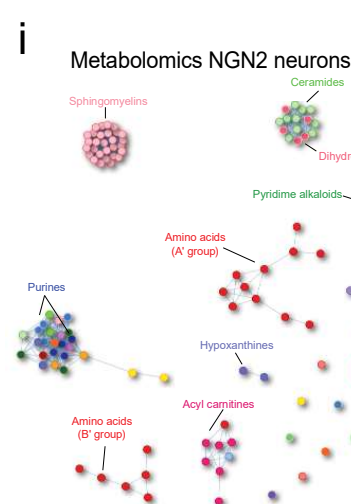
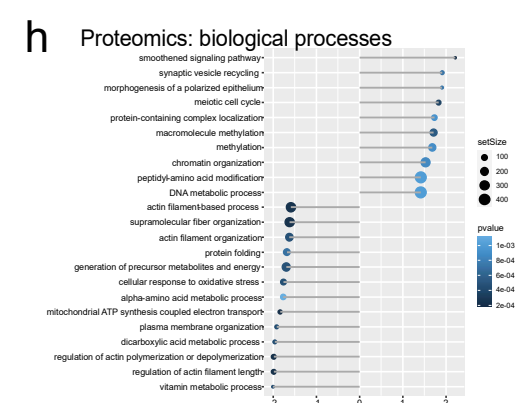
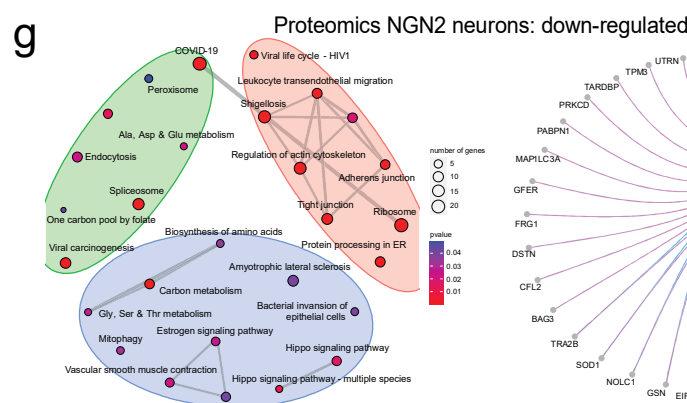
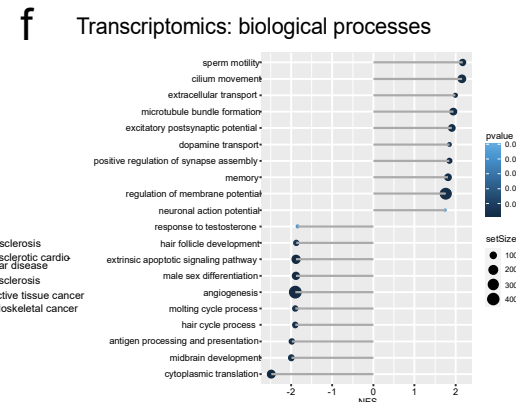
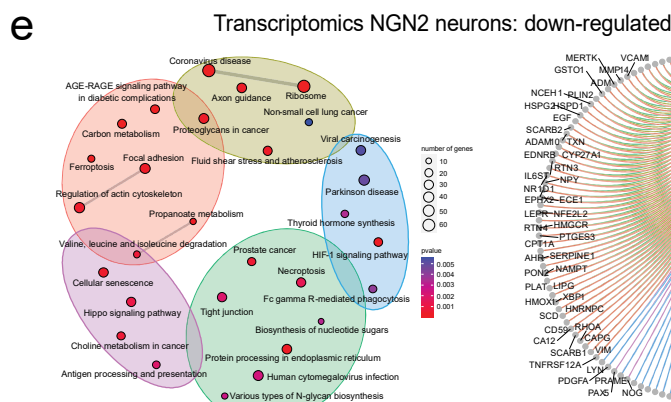
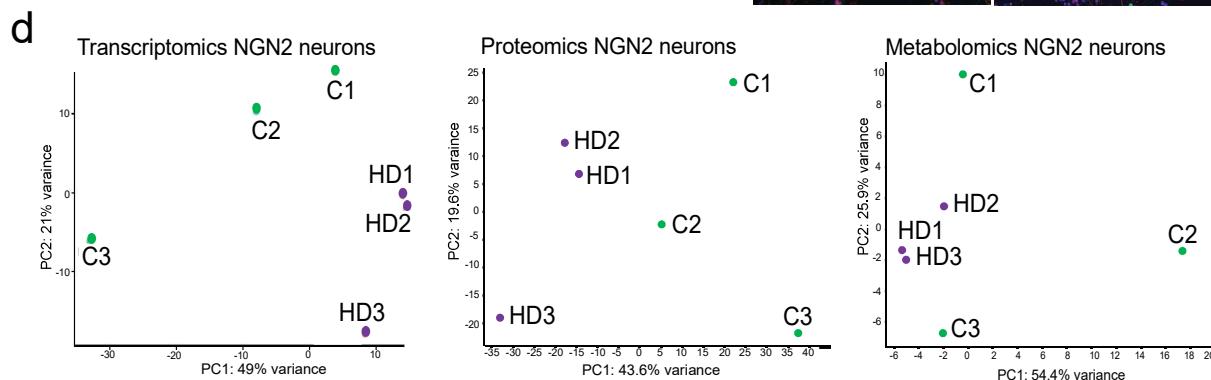
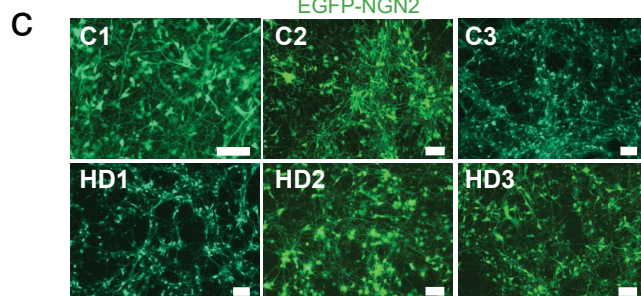
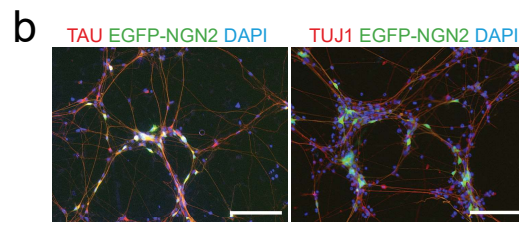
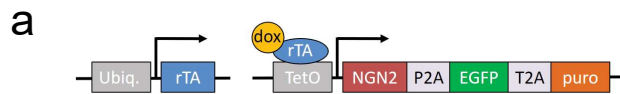
Supplementary Fig. 4. Transcriptional signatures of engineered mHTT cells across different neurodevelopmental stages (related to Fig. 3). **a** Venn diagram of unique and common transcripts among iPSCs, NPCs, cerebral organoids (COs) at day 28, and COs at day 49. **b** Heatmap of log-fold change (LFC) comparisons of differential gene expression of the 47 transcripts in common across all neurodevelopmental stages in 70/70Q cells compared to WT/WT cells. **c-d** Heatmap of the normalized expression values (TPM: Transcripts Per Million) of transcripts belonging to the GO category of “nucleic acid binding” and “nervous system development”. **e-f** Representative immunoblot and related quantification of CHCHD2 expression and beta actin in NPCs. n=3 independent biological replicates (dots) per line; *p<0.05; ns: not significant; unpaired two-tailed Welch t test.



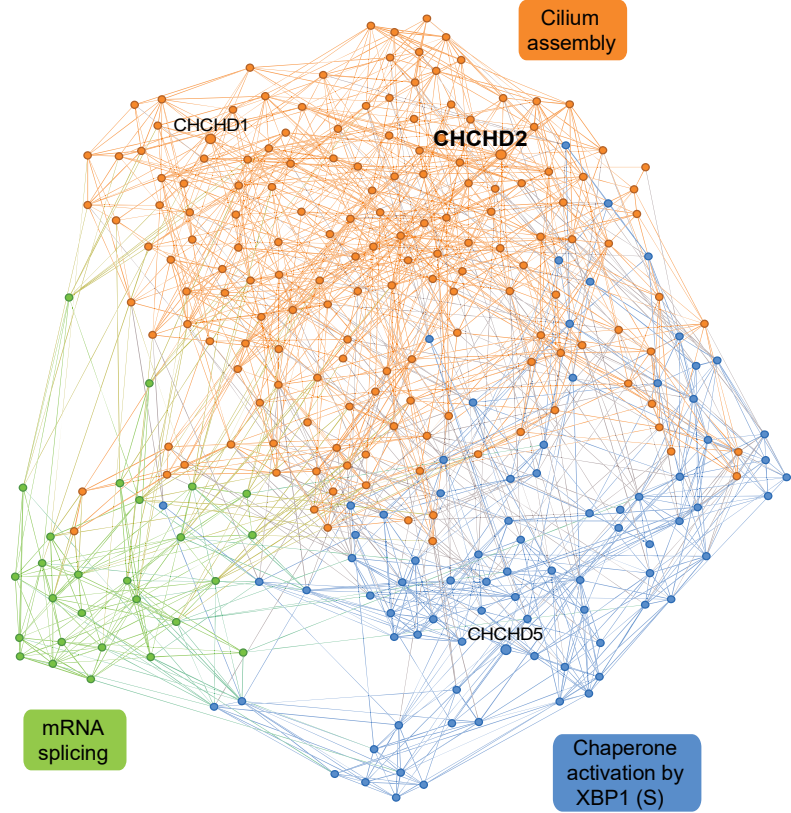
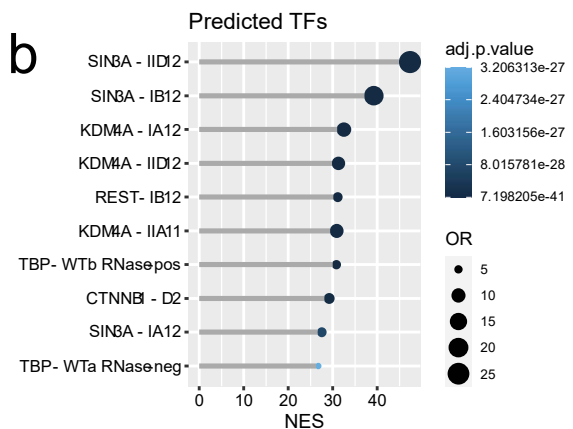
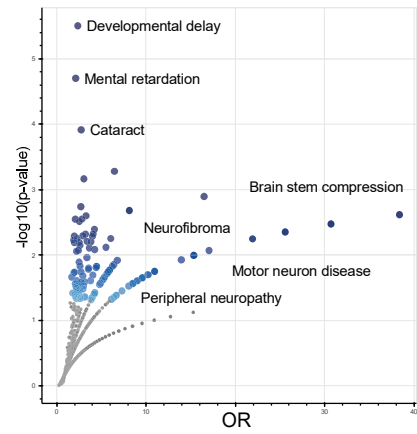
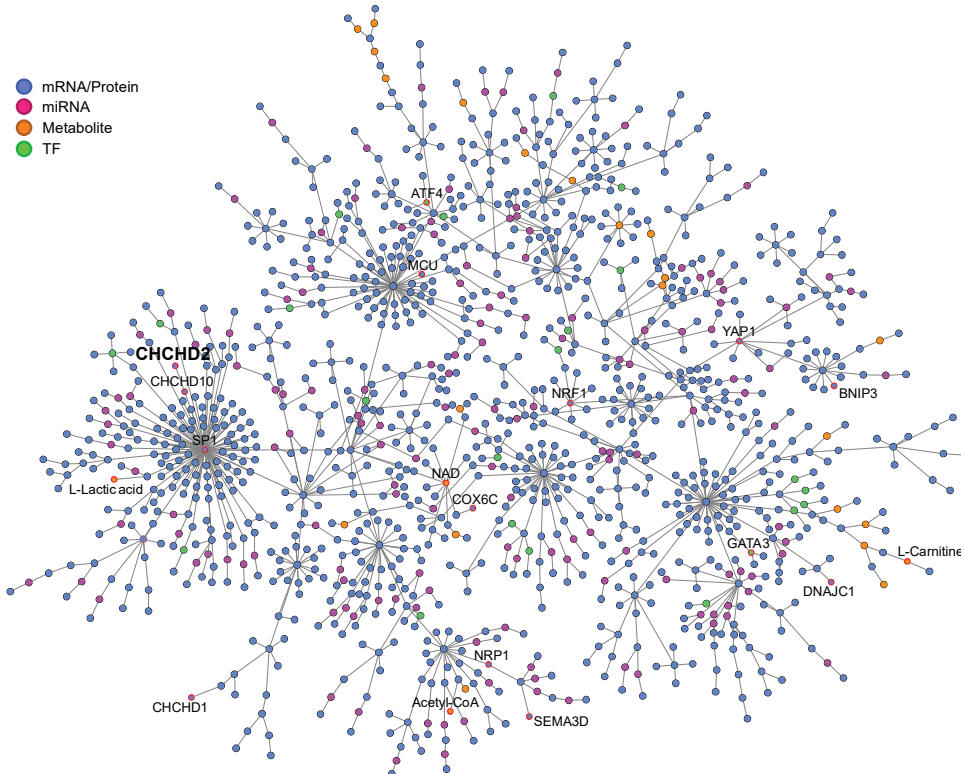
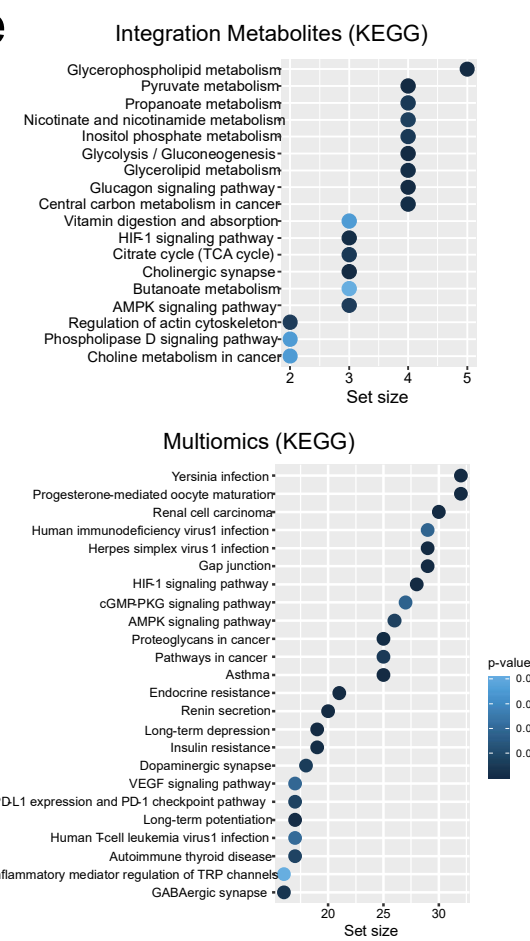
Supplementary Fig. 5. Mitochondria morpho-dynamics changes in neural cells carrying mHTT (related to Fig. 4 and Fig. 5). **a** Representative images of midbrain organoids from WT/WT and 70/70Q stained with CHCHD2. Data were repeated in two independent experiments. Scale bar: 100 μ m. **b-d** Long-read sequencing analysis showing the distribution of the recognized variants classified by structural categories, the number of isoforms detected, and the distribution of number of isoforms per gene in WT/WT NPCs and 70Q/70Q NPCs. **e** Heatmap of log-fold change (LFC) comparisons of genes involved in mitochondrial biogenesis, mitochondrial quality control, and senescence based on bulk RNA sequencing from iPSCs, NPCs, and cerebral organoids (COs) derived from 70Q/70Q. HD neuruloids were compared to WT neuruloids. **f** Quantification of immunostaining for mitochondrial footprint of small mitochondrial structures (<0.5 μ m) and large mitochondrial structures (>0.5 μ m) based on TOM20 signal in cerebral organoids from 70Q/70Q and WT/WT. Dots represent individual images collected over three independent experiments (AU=arbitrary units). * $p<0.05$, ** $p<0.01$, *** $p<0.001$, ns: not significant; unpaired two-tailed Welch t test. **g** Quantification of mitochondrial roundness and mitochondrial area based on electron microscope images. Each dot represents an individual mitochondrion from NPCs measured in two biological replicates per line (AU=arbitrary units). ** $p<0.01$, ns: not significant; unpaired two-tailed Welch t test.



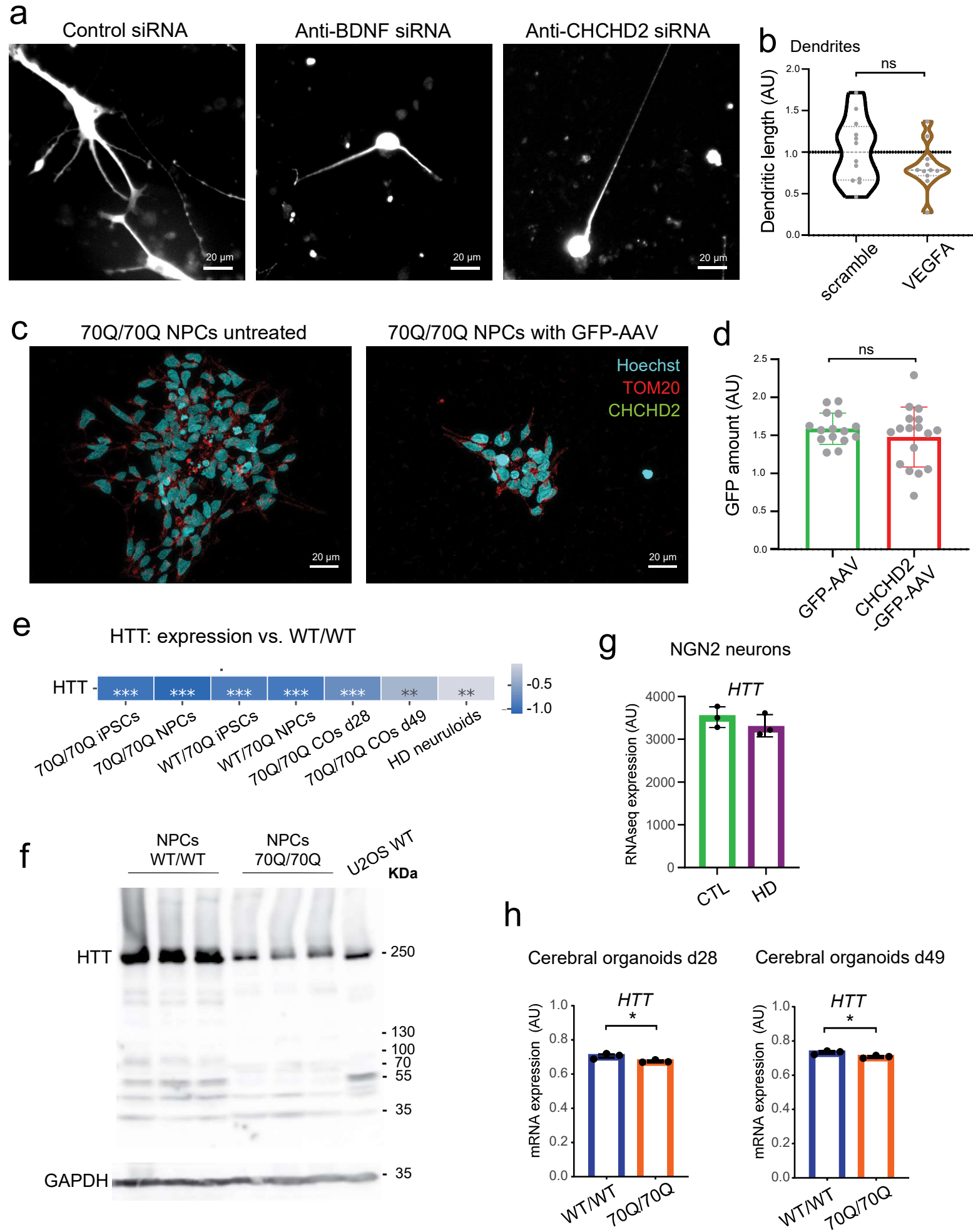
Supplementary Fig. 6. Disruption of metabolism and mitochondrial respiratory chain complexes in iPSCs and NPCs carrying mHTT (related to Fig. 5). **a** Relative glucose utilization at resting energy demands in iPSCs from WT/WT and 70Q/70Q based on proteomics-driven functional metabolic analysis. **b** Gene set enrichment analysis (GSEA) showing decreased oxidative phosphorylation (OXPHOS) and increased glycolysis/gluconeogenesis in 70Q/70Q iPSCs compared to WT/WT iPSCs. **c** Proteomics-driven functional metabolic analysis depicting the substrate utilization at maximal energy demands of iPSCs from WT/WT and 70Q/70Q. Energetic capacities were evaluated by computing the changes of metabolic state elicited by an increase of the ATP consumption rate above the resting value. Bar graphs show consumption of glucose (gluc) and production of lactate-pyruvate (lact/pyr). **d-e** Metabolic state variables for NAD/NADH ratio and mitochondrial NAD/NADH ratio in iPSCs from WT/WT and 70Q/70Q in dependence of increasing energetic demands. **f-g** Computed ATP/ADP ratio in dependence of increasing energetic demands and maximal ATP production capacity in iPSCs from WT/WT and 70Q/70Q. **h** Representative blue native PAGE of mitochondrial complex assembly in WT/WT NPCs, 70Q/70Q NPCs, and 0Q/0Q NPCs. n=3 independent biological replicates per line run in two different blots. **i-j** Heatmap of log fold change (LFC) comparisons of genes involved in mitochondrial respiratory chain composition and assembly based on bulk RNA sequencing performed in iPSCs, NPCs, and COs from 70Q/70Q and WT/70Q compared to WT/WT. HD neuruloids were compared to WT neuruloids.



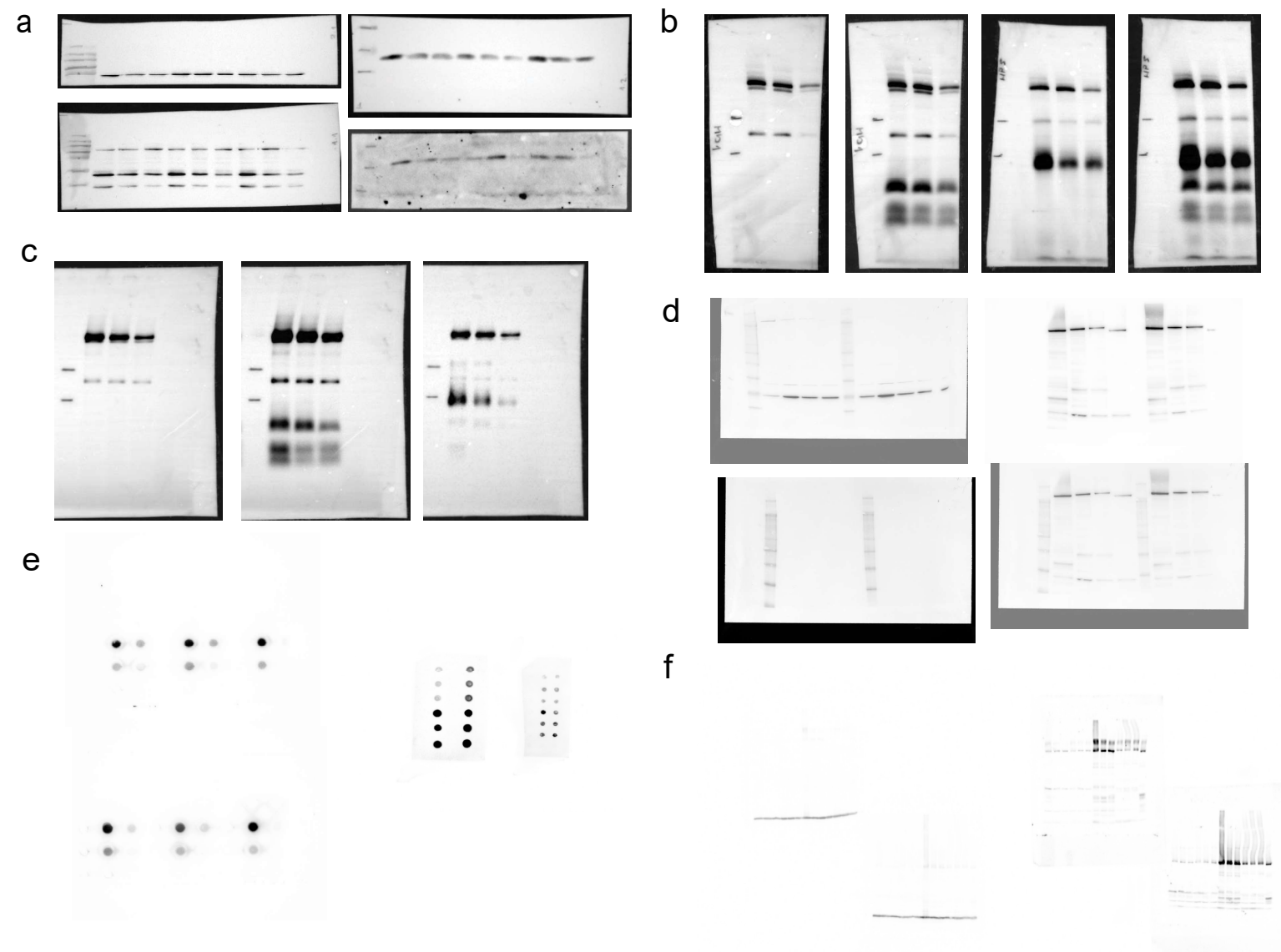
Supplementary Fig. 7. Characterization and multi-omics analysis of NGN2 neurons from three healthy controls and three individuals with HD (related to Fig. 6). **a** Lentiviral constructs used for transducing NPCs for NGN2 neuron derivation. **b** Expression of neuronal and synaptic markers in NGN2 neurons at day 14 of differentiation from NPCs (C1 line). Data were repeated in three independent experiments. Scale bar: 100 µm. **c** NGN2 neurons at day 14 of differentiation from healthy controls (C1, C2, C3) and individuals with HD (HD1, HD2, HD3). Data were repeated in three independent experiments. **d** Principal component analysis (PCA) plots showing the distribution of the NGN2 neurons from healthy controls (C1, C2, C3) and individuals with HD (HD1, HD2, HD3) based on transcriptomics, proteomics, and metabolomics. **e** Transcriptomics analysis of NGN2 neurons. Left: over-representation analysis (ORA) of downregulated DEGs for KEGG pathways; right: ORA of downregulated DEGs for human diseases. **f** GSEA for affected GO biological processes (BPs) (NES: normalized enrichment score). **g** Proteomics analysis of NGN2 neurons. Left: ORA of downregulated DEPs for KEGG pathways; right: ORA of downregulated DEPs for human diseases. **h** GSEA for affected GO BPs (NES: normalized enrichment score). **i** Metabolomics analysis of NGN2 neurons. Structure similarity analysis grouping of the dysregulated metabolites based on their family hierarchy. **j** ORA of DEMs for affected metabolic pathways in multiple databases. **k** Oxygen consumption rate (OCR) profile obtained with Seahorse Bioanalyzer in NGN2 neurons from healthy controls (C1, C2, C3) and individuals with HD (HD1, HD2, HD3). Mean +/- s.e.m.; n=3 independent biological replicates per line.

a**b****c****d****e**

Supplementary Fig. 8. Multi-omics integration of NGN2 neurons (related to Fig. 7). **a** Protein co-expression network in NGN2 neurons showing the biggest cluster of co-expressed proteins ($n=272$) including CHCH domain-containing proteins (CHCHD1, CHCHD2, CHCHD5). Three modules were generated by breaking the network into communities of densely connected proteins. Enrichment analysis for REACTOME pathways indicated that they are associated with cilium assembly, chaperone activation by XBP1(S) and mRNA splicing. **b** Enrichment analysis for upstream transcription factors of the 272 co-expressed proteins (NES: normalized enrichment score). **c** ORA of 272 co-expressed proteins for human diseases in the GeDiPNet database (OR: odds ratio). **d** Multi-omics integration of NGN2 neurons. Network of significantly dysregulated transcripts, proteins and metabolites along with predicted intermediate miRNAs and transcription factors. **e** Top: enrichment analysis of metabolites included in the multi-omics network. Bottom: enrichment analysis of all entities that participate in the multi-omics network.



Supplementary Fig. 9. Manipulation of CHCHD2 expression in neural cells (related to Fig. 7). **a** Representative images of NGN2 neurons directly generated from the healthy inducible iPSC line BIHi005-A visualized at day 17, four days after transfection with different siRNA constructs. NGN2 neurons transfected with scramble control siRNA exhibit multiple neurite branching, while these were diminished in NGN2 neurons transfected with siRNA against BDNF or CHCHD2. Data were repeated in three independent experiments. **b** Quantification of neuronal arborization assessed by high-content imaging based on antibodies labeling dendrites (MAP2) at day 17, two days after transfection with either control scramble siRNA or siRNA against VEGFA. Dot indicates different replicates out of two independent experiments. ns: not significant; unpaired two-tailed Welch t test. **c** Representative images of 70Q/70Q NPCs at basal condition or after transduction with GFP-AAV showing similar level of TOM20 and CHCHD2 expression. Data were repeated in two independent experiments. **d** Quantification of GFP signal amount in 70Q/70Q NPCs transduced with either GFP-AAV or CHCHD2-GFP-AAV. Dots represent individual images collected from two independent experiments. ns: not significant; unpaired two-tailed Welch t test. **e** Heatmap of log-fold change (LFC) comparisons of *HTT* gene based on bulk RNA sequencing performed in iPSCs, NPCs, and COs from 70Q/70Q and WT/70Q compared to WT/WT. HD neuruloids were compared to WT neuruloids. **f** Representative immunoblot of wild-type HTT in NPCs from WT/WT and 70Q/70Q. The results were confirmed in two independent experiments. **g** *HTT* expression based on RNA sequencing in NGN2 neurons derived from controls (C1, C2, C3) and individuals with HD (HD1, HD2, HD3) (AU=arbitrary units). **h** qPCR-based *HTT* expression in unguided cerebral organoids at day 28 and 49. Mean +/- s.e.m.; n=3 independent biological replicates (dots) per line (AU=arbitrary units); *p<0.05 **p<0.01; unpaired two-tailed t test. Four organoids were pooled for each individual RNA isolation.



Supplementary Fig. 10. Original blots (related to Fig. 5, Supplementary Fig. 1, Supplementary Fig. 2, Supplementary Fig. 6, Supplementary Fig. 9). **a** Unprocessed blot scans related to Fig. 5g. **b** Unprocessed blot scans related to Fig. 5i. **c** Unprocessed blot scans related to Supplementary Fig. 6h. **d** Unprocessed blot scans related to Supplementary Fig. 1b. **e** Unprocessed blot scans related to Supplementary Fig. 2c. **f** Unprocessed blot scans related to Supplementary Fig. 9f.